Physics Communication
Volume 10 Issue 1 Year 2026 Pages 37-49

P-ISSN 2528-5971 | E-ISSN 2528-598X
https://journal.unnes.ac.id/journals/pc
https://doi.org/10.15294/pc.v10i1.45531

Comparison of Physics-Informed Neural Networks (PINNs) and Experimental Reality in Fluid Viscosity Dynamics

Elgana Septiana*, Joko Saefan, Joko Siswanto

Physics Education Study Program, Faculty of Mathematics, Natural Sciences, and Information Technology, Universitas PGRI Semarang, Indonesia

*Correspondence to: *septianaelgana@gmail.com*

Abstract: Determining fluid viscosity using the conventional falling-sphere method is frequently confronted with challenges related to experimental variability and measurement instrument limitations. As an alternative, Physics-Informed Neural Networks (PINNs) offer a computational approach capable of integrating physical laws into the neural network architecture. This study aims to evaluate the predictive accuracy of the PINNs model regarding the velocity of a falling sphere, as well as to compare it with the analytical solution of Stokes flow and experimental data. Data collection was conducted using a viscometer equipped with five infrared sensors, while the PINNs model was trained by balancing the experimental data loss and the physics loss derived from the equation of motion. The comparative results demonstrate that PINNs generally succeed in modeling the dynamics of the sphere's motion, convergently reaching terminal velocity. Nevertheless, two primary modeling limitations were identified. First, the model experiences an overshoot during the initial phase of motion due to the network's spectral bias effect when responding to drastic velocity changes. Second, the experimental data reveal a persistent velocity deceleration in the final phase that both the analytical and PINNs predictions failed to capture. This empirical anomaly indicates the occurrence of a shift in boundary-layer separation alongside the thixotropic effects of the fluid. In conclusion, PINNs prove to be a promising approach for bridging the gap between computational modeling and experimentation; however, this architecture still requires the inclusion of dynamic parameters to fully accommodate the complexity of fluids under real-world conditions.

Keywords: Fluid Dynamics; Physics-informed Neural Networks; Machine Learning; Viscosity

Submitted: 2025-12-20. **Revised:** 2026-01-03. **Accepted:** 2026-02-09.

Introduction

Viscosity is a physical parameter that indicates how strongly a fluid resists deformation when subjected to shear stress. Cohesive forces between adjacent fluid molecules create internal friction as they move past each other. This fundamentally affects the behavior of fluid flow under various applied forces. This parameter plays a fundamental role in both fundamental physics and various engineering fields, ranging from fluid transportation in pipelines to materials engineering and biomedical systems (White, 2011). For example, in biomedical engineering, precise fluid resistance modeling is crucial for designing artificial cardiovascular systems. Meanwhile, in the manufacturing industry, it affects the amount of energy required to pump highly viscous materials, such as crude oil or polymers (White & Xue, 2021). Furthermore, in the realm of fundamental physics, viscosity is a critical parameter for understanding complex phenomena such as the settling dynamics of atmospheric aerosols or mantle convection in geophysics (Beuchert & Podladchikov, 2010). In the context of particle motion within a fluid, the dynamics of a sphere are generally described by Stokes' law. This law states that the drag force is directly proportional to the particle's radius, its velocity, and the fluid's viscosity (Mendez, 2011; Salomone et al., 2018). Stokes' theory works only under the assumption of creeping flow, which occurs at very low Reynolds numbers. Under these conditions, viscous forces are very strong compared to inertial forces. This results in a predictable and symmetric hydrodynamic field around the object. This principle forms the basis of the falling-sphere viscometer method, in which viscosity is determined by measuring the terminal velocity of a sphere moving through the fluid (Akhlis et al., 2020; Mitev et al., 2025). Reaching this terminal velocity means that the system is in dynamic equilibrium. The downward force of gravity is balanced by the combined buoyancy force of the fluid and the upward force of viscous drag. Consequently, the accuracy of viscosity determination relies heavily on the precision of the mathematical modeling and the parameters utilized.

Determining viscosity experimentally is often fraught with various challenges. Frequently encountered issues include instrument calibration errors, sensitivity to temperature and pressure fluctuations, limited device resolution, and human error, all of which can compromise measurement accuracy (Brizard et al., 2005). Furthermore, there are additional physical constraints in laboratory settings, such as the wall effect, which disrupts the ideal flow pattern around the object (Akhyan et al., 2025). When an object is too close to the tube wall, it causes an asymmetric velocity gradient, which unnaturally increases the drag force on the ball. This phenomenon requires complex mathematical calculations—such as Faxén's law—and is often not perfectly quantifiable in practice (Chu et al., 2024). Another prevalent difficulty lies in maintaining the initial release position of the sphere along the centerline of the tube. The sphere often tends to move eccentrically away from the tube's center (the eccentricity effect), altering the magnitude of the drag force and accelerating its descent (Rückert et al., 2023). These deviations often occur due to small imperfections on the surface of the sphere, slight inaccuracies in the vertical placement of the measuring instrument, or due to the formation of an asymmetrical flow pattern in the fluid column. Moreover, conducting experiments with fluids exhibiting complex characteristics is frequently costly and time-consuming (Barnes et al., 1989). Repeated physical tests require very careful cleaning procedures, large numbers of chemical samples that can be expensive or risky, and extensive experimentation on a variety of factors to obtain statistically reliable results. These variations in experimental data underscore the necessity for alternative methods that enhance efficiency while preserving accuracy.

The advancement of artificial intelligence has unlocked new opportunities in the modeling of physical systems. One rapidly emerging approach is Physics-Informed Neural Networks (PINNs). PINNs effectively narrow the space of admissible solutions by integrating physical laws, formulated as differential equations, into the neural network's training process utilizing automatic differentiation. This mechanism ensures that the network's outputs remain strictly consistent with the governing physical laws. Through this method, the model learns not only from available empirical data but also from the underlying mathematical structure of the physical system (Raissi et al., 2019). PINNs possess the potential to yield more consistent predictions regarding the behavior of dynamic systems compared to purely data-driven models. Standard machine learning algorithms often fail to generalize well beyond the existing training data and can even produce physically impossible predictions. Previous studies have demonstrated the advantages of PINNs over purely data-driven models. For instance, Karniadakis et al. (2021) emphasized that conventional machine learning models often fail to generalize beyond training datasets and may produce physically inconsistent results (Karniadakis et al., 2021). In contrast, Cuomo et al. (2022) showed that PINNs significantly reduce the need for large datasets by embedding physical constraints, while Fowler et al. (2024) successfully applied PINNs to fluid-related problems with improved stability and accuracy (Cuomo et al., 2022; Fowler et al., 2024). However, these studies are predominantly conducted within controlled or idealized computational environments, where experimental uncertainties and real-world disturbances are not explicitly considered. In the context of fluid viscosity and falling-sphere dynamics, existing studies have not sufficiently addressed the discrepancy between computational predictions and experimental observations. In particular, the influence of experimental noise, near-wall effects, and potential non-Newtonian behaviors remains underexplored in PINNs-based modeling. Most PINNs implementations assume steady, homogeneous Newtonian fluids, which may not adequately represent real experimental conditions. Therefore, this study compares PINNs predictions with experimental data, utilizing the analytical solutions as a theoretical baseline. This approach not only evaluates the predictive capability of PINNs but also investigates their potential role as a diagnostic tool for identifying physical anomalies that deviate from ideal theoretical assumptions.

PINNs operate by utilizing an artificial neural network architecture that incorporates multiple physical constraints and latent variables, computed purely mathematically within an idealized space. In this environment, factors such as fluid conditions, spherical shape, and temperature are assumed to be perfectly constant and immune from external disturbances. In contrast, experiments reflect true physical reality, replete with practical challenges in laboratory setups and fluctuating environmental conditions (Karniadakis et al., 2021). In reality, experimental conditions are often affected by unsteady fluid flow disturbances, making it impossible to achieve perfect mathematical conditions.

This study aims to analyze the determination of terminal velocity using the PINNs method as a representation of computational abstraction against experimental results, which represent reality, in the context of fluid viscosity. It is anticipated that this comparative analysis will illuminate the boundaries of computational capabilities and the inherent complexity of actual physical reality.

Theoretical Framework

Viscosity of Newtonian Fluids

A Newtonian fluid is defined as a fluid that maintains a constant viscosity independent of the shear rate. Mathematically, the relationship between shear stress and the velocity gradient is expressed through Newton's law of viscosity, namely:

$$\tau = \mu \frac{du}{dy} \tag{1}$$

Where $\boldsymbol{\tau}$ is the shear stress, $\boldsymbol{\mu}$ is the dynamic viscosity, and $\boldsymbol{\frac{du}{dy}}$ is the velocity gradient perpendicular to the direction of flow. This equation is known as Newton's law of viscosity, stating that shear stress is directly proportional to the rate of deformation. This linear relationship serves as the foundation in fluid flow modeling, as it allows viscosity to be treated as a material constant within a specific range of conditions (Kaliappan et al., 2022).

Falling Sphere in a Fluid

Under the condition of $Re \ll 1$, the flow is characterized as Stokes flow, where viscous forces dominate over inertial forces (Khain et al., 2022; Protopapas et al., 2025). In this regime, the dynamics of a spherical particle falling through a fluid are governed by the equilibrium of three primary forces: gravitational force (weight), buoyancy force, and viscous drag force. See Figure 1.

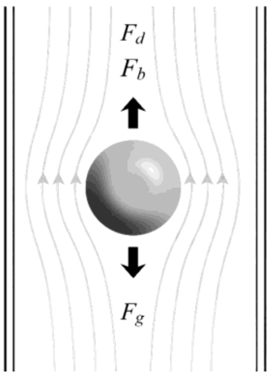

Figure 1. Free body diagram of a spherical particle in a viscous fluid

The gravitational force acting on the particle is expressed as:

$$F_g = \rho_s V g \tag{2}$$

The buoyancy force is given by:

$$F_b = \rho_f V g \tag{3}$$

and the Stokes drag force is:

$$F_d = 6\pi\mu r v \tag{4}$$

where F_g is the gravitational force, F_b is the buoyancy force, F_d is the Stokes drag force, ρ_s and ρ_f are the densities of the sphere and the fluid respectively, V is the volume of the sphere, g is the gravitational acceleration, μ is the dynamic viscosity of the fluid, r is the radius of the sphere, and v is the velocity of the sphere.
By applying Newton's second law, the equation of motion is obtained:

$$m\frac{dv}{dt} = F_g - F_b - F_d \tag{5}$$

$$m\frac{dv}{dt} = (\rho_s - \rho_f)Vg - 6\pi\mu r v \tag{6}$$

Since the mass of the particle is:

$$m = \rho_s V \tag{7}$$

Thus, the equation of motion can be explicitly written as:

$$\rho_s V\frac{dv}{dt} = (\rho_s - \rho_f)Vg - 6\pi\mu r v \tag{8}$$

By substituting the sphere volume $V = \frac{4}{3}\pi r^3$ into Equation (8) and simplifying the geometric terms, the governing equation can be expressed in a more computationally efficient form as follows:

$$\frac{dv}{dt} = \left(1 - \frac{\rho_f}{\rho_s}\right)g - \frac{9\mu}{2\rho_s r^2}v \tag{9}$$

This equation will serve as the foundation for deriving the analytical solution and will be utilized as the physical equation embedded within the physics loss function in the Physics-Informed Neural Networks method.

Analytical Solution

By restructuring the simplified equation of motion, the dynamics of the falling sphere can be expressed as a standard first-order linear ordinary differential equation (White, 2011):

$$\frac{dv}{dt} = A - Bv \tag{10}$$

where the constant coefficients are defined based on the physical properties of the system:

$$A = \left(1 - \frac{\rho_f}{\rho_s}\right)g, \quad B = \frac{9\mu}{2\rho_s r^2} \tag{11}$$

Physically, the constant A represents the effective gravitational acceleration acting on the sphere (attenuated by the fluid's buoyancy), while the parameter B serves as the viscous damping frequency, dictating how rapidly the fluid resistance reacts to the particle's motion.
Solving this differential equation yields the velocity profile as a function of time, revealing the transition from initial acceleration to a steady state:

$$v(t) = v_t(1 - e^{-Bt}) \tag{12}$$

where the terminal velocity (v_t) represents the theoretical equilibrium state when the effective gravity is perfectly balanced by the viscous drag force ($A = Bv_t$):

$$v_t = \frac{A}{B} = \frac{2r^2 g(\rho_s - \rho_f)}{9\mu} \tag{13}$$

The spatial trajectory of the particle is subsequently obtained by integrating the velocity function over time:

$$x(t) = \int v(t)\, dt \tag{14}$$

yielding the exact analytical position function:

$$x(t) = v_t t + \frac{v_t}{B}(e^{-Bt} - 1) \tag{15}$$

From a physical perspective, Equation (15) elegantly illustrates that the sphere's total displacement is composed of two distinct components: a steady-state linear descent governed by $v_t t$, and a transient spatial lag induced by the fluid's initial inertia and viscous resistance, represented by the exponential term.

Physics-Informed Neural Networks (PINNs)

Theoretical Basis of Machine Learning

Machine learning (ML) is a branch of artificial intelligence that enables models to learn patterns from data through the optimization of a loss function. In the context of regression, an artificial neural network (ANN) is utilized to map the relationship between inputs and outputs through a composition of linear and nonlinear transformations. Generally, a neural network consists of an input layer, hidden layers, and an output layer (see Figure 2). The input layer receives the input variables (in this study, time t), the hidden layers perform nonlinear transformations on the data, while the output layer generates predictions, such as $v(t)$ or $x(t)$.

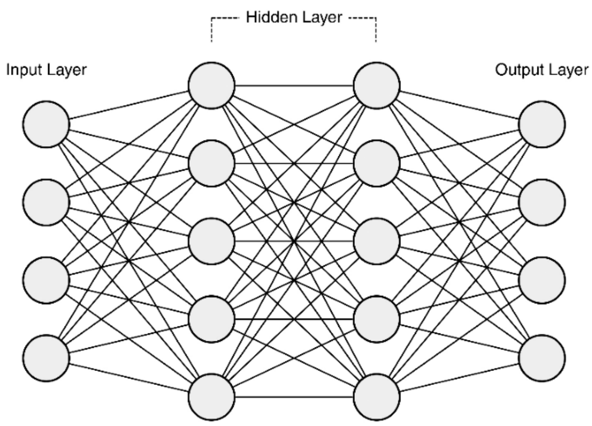

Figure 2. Schematic diagram of a multilayer perceptron ANN architecture

Every neuron within the network performs a linear combination operation $z = Wx + b$, which is subsequently passed through a nonlinear activation function to produce an output $a = \sigma(z)$, where W represents the weights, b is the bias, and σ is the activation function. The activation function plays a role in introducing nonlinearity into the model. Several commonly utilized functions include sigmoid, tanh, ReLU, and Swish. In the modeling of differential systems, smooth activation functions such as tanh are frequently selected due to their continuous derivatives, thereby facilitating the process of automatic differentiation. In conventional approaches, ANNs are trained by minimizing the error between predictions and observational data, without explicitly accounting for the physical laws underlying the modeled system (Goodfellow et al., 2016; Karniadakis et al., 2021).

The Concept of Physics-Informed Neural Networks (PINNs)

Physics-Informed Neural Networks (PINNs) are a machine learning approach that integrates physical laws, in the form of differential equation residuals, into the neural network's loss function. Consequently, the resulting model remains consistent with the underlying physical laws (Fowler et al., 2024; Ren et al., 2025). Assuming the network approximation function for velocity is denoted as $v_\theta(t)$, then based on the governing Equation (10), the physics residual for the falling sphere system is formulated in its first-order form as:

$$\mathcal{R}(t) = \frac{dv_\theta}{dt} - (A - Bv_\theta) \tag{16}$$

The physics loss is then defined as:

$$\mathcal{L}_{physics} = \frac{1}{N_f}\sum_{i=1}^{N_f} \mathcal{R}(t_i)^2 \tag{17}$$

If the model fully satisfies the physical laws, the residual will approach zero across the entire time domain. The data loss measures the error between the model's predictions and the experimental data:

$$\mathcal{L}_{data} = \frac{1}{N_d}\sum_{i=1}^{N_d} | v_\theta(t_i) - v_i^{exp} |^2 \tag{18}$$

or, if using position data:

$$\mathcal{L}_{data} = \frac{1}{N_d}\sum_{i=1}^{N_d} | x_\theta(t_i) - x_i^{exp} |^2 \tag{19}$$

The total loss function is a combination of both:

$$\mathcal{L}_{total} = \mathcal{L}_{data} + \lambda\mathcal{L}_{physics} \tag{20}$$

with λ acting as a weighting parameter that controls the contribution of the physical constraints.

Error Metrics

To evaluate the model's performance, the following metrics are utilized:

Mean Squared Error (MSE)

$$\mathrm{MSE} = \frac{1}{\mathrm{N}}\sum_{\mathrm{i}=1}^{\mathrm{N}}\left(\mathrm{v}_\mathrm{i}^{\mathrm{pred}} - \mathrm{v}_\mathrm{i}^{\mathrm{exp}}\right)^2 \tag{21}$$

Root Mean Squared Error (RMSE)

$$\mathrm{RMSE} = \sqrt{\mathrm{MSE}} \tag{22}$$

as well as the global L2 norm:

$$\left\|\mathrm{v}_{\mathrm{pred}} - \mathrm{v}_{\mathrm{exp}}\right\|_2 = \sqrt{\sum_{\mathrm{i}=1}^{\mathrm{N}}\left(\mathrm{v}_\mathrm{i}^{\mathrm{pred}} - \mathrm{v}_\mathrm{i}^{\mathrm{exp}}\right)^2} \tag{23}$$

RMSE provides an error interpretation in the same physical units as the measured variable, thereby facilitating easier comparison with experimental results.

Methods

Research Design

This study employs an experimental approach alongside computational modeling based on Physics-Informed Neural Networks (PINNs) to analyze the motion dynamics of a falling sphere in a viscous fluid. The research workflow encompasses the acquisition of falling sphere velocity data, the formulation of a physical model based on Stokes flow, the implementation and training of a neural network embedded with physical constraints, and the evaluation of the model's performance utilizing the Root Mean Squared Error (RMSE) metric.

Experimental Design

The experiment was conducted using a 50 cm tall transparent tube equipped with five calibrated infrared (IR) sensors possessing a minimum scale resolution of 0.01 s (see Figure 3). These sensors were strategically installed at uniform 10 cm intervals along the tube's wall. This equidistant placement ensures a consistent spatial resolution, allowing the sphere's velocity to be calculated segmentally between each sensor interval rather than from a single initial starting point. Furthermore, the first sensor was intentionally positioned slightly below the fluid's surface. This design choice was implemented to allow the sphere to fully submerge and to mitigate disturbances caused by surface tension and initial entry impact, ensuring that the initial time measurement ($t = 0$) begins only after the interfacial turbulence has dissipated and interfaced with an Arduino Uno microcontroller to automatically record the travel time. The test object utilized was a sphere with a precisely calibrated mass specification of 5.64 g to ensure the reliability of the gravitational and buoyancy force calculations.

The physical parameters of the fluid and the particle were set according to the details in Table 1, where the particle's theoretical terminal velocity (0.096 m/s) was analytically projected referring to Equation (13). Meanwhile, the extracted experimental dataset (presented in Table 2) represents the average values obtained from five experimental repetitions. The empirical velocity at each time point was calculated observationally by dividing the fixed 0.1 m distance between each sensor interval by the recorded travel time, thus capturing the changing dynamics before reaching equilibrium. To enhance the stability of the computational training process, the time variable was normalized against the maximum observation time, $t_{max} = 6\ s$.

Table 1. Physical parameters of the fluid and spherical particle

Parameter	Value
Sphere radius (r)	0.010125 m
Sphere mass (m)	0.00564 kg
Sphere density (ρ_s)	1297.2 kg/m³
Fluid glycerin density (ρ_f)	1000 kg/m³
Fluid glycerin viscosity (μ)	0.69 Pa·s
Gravitational acceleration (g)	9.81 m/s²

Table 2. Experimental time and velocity data

t (s)	v (m/s)
0.00	0.000
0.7696	0.1299
1.6808	0.1097
2.713	0.0968
5.1562	0.0920

The dynamic viscosity value $\mu = 0.69$ Pa·s was determined analytically using the standard Stokes' falling-sphere equation derived from Equation (13)

Computation of Physics-Informed Neural Networks

The PINNs model was constructed using a feed-forward neural network that maps time to particle velocity. The network approximation function is denoted as $v_\theta(t)$, where θ represents the network parameters.

Table 3. Configuration of the PINNs architecture

Neural Network	Configuration
Input layer	1 neuron (time variable t)
Hidden layers	3 hidden layers
Number of neurons per layer	64
Activation function	Hyperbolic tangent (tanh)
Output layer	1 neuron (velocity)

Mathematically, the neuron operation at each layer can be expressed as:

$$z^{(l)} = \sigma(W^{(l)} z^{(l-1)} + b^{(l)})$$

where $W^{(l)}$ denotes the network weights, $b^{(l)}$ is the bias, and $\sigma(\cdot)$ represents the tanh activation function.

To ensure consistency with the system's initial conditions, the model applies a hard constraint $v(0) = 0$, which is implemented by defining the network output as $v_\theta(t) = t \cdot N_\theta(t)$ where $N_\theta(t)$ is the output of the neural network. This approach guarantees that the model's solution automatically satisfies the initial condition. To esnforce the physical laws within the time domain, collocation points randomly sampled within the normalized computational time interval $t_{\text{norm}} \in [0,1]$ were utilized. This normalized interval corresponds linearly to the actual physical experimental time domain of $t_{\text{phys}} \in [0,6]$ s, utilizing the scaling transformation $t_{\text{norm}} = \frac{t_{\text{phys}}}{t_{\text{max}}}$. This normalization strategy was strictly implemented to ensure numerical stability and accelerate convergence during the neural network training process. A total of $N_f = 2000$ collocation points were used to compute the differential equation residuals.

The optimized total loss function is a combination of the physics loss and the data loss (as defined in Equations 17 and 18), with the application of a weighting parameter $\lambda = 10$ to amplify the contribution of fidelity to the experimental data. The neural network training was conducted using the Adam optimization algorithm with a learning rate of 10^{-3}. The training process was executed for 5000 epochs until the loss function achieved convergence. The final evaluation of the PINNs model's accuracy against the analytical solution and experimental data was quantitatively measured using the RMSE metric. A smaller RMSE value indicates a higher degree of agreement between the PINNs model and the analytical solution.

Results and Discussion

In alignment with the study's primary objective to contrast computational modeling with physical reality, the prediction results of the Physics-Informed Neural Networks (PINNs)—computed by optimizing the loss functions defined in Equations (17) and (18)—were systematically compared against the empirical experimental data. The theoretical analytical solution (Equation 12) is incorporated into this analysis strictly as an idealized mathematical baseline to contextualize the deviations. The comparative analysis, as illustrated in the velocity profile (Figure 4), reveals two distinct phenomena: an algorithmic deviation in the PINNs model during the early phase, and a physical anomaly in the experimental data during the later phase.

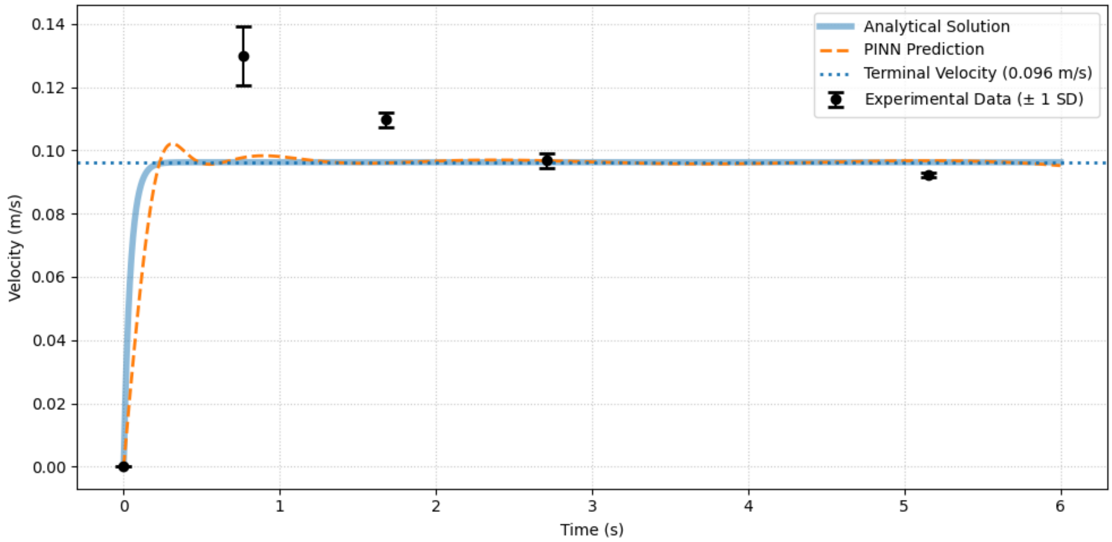

Figure 4. Velocity profile comparison: PINNs vs experimental and analytical data

It is important to emphasize upfront that while the computational and analytical models successfully converge to the theoretical terminal velocity, the experimental data notably diverges by exhibiting a continuous deceleration. This specific empirical anomaly will be addressed and analyzed in detail in the subsequent sections.

Regarding the initial phase, the PINNs prediction curve experiences an overshoot relative to the analytical baseline before ultimately converging toward the terminal velocity condition. Quantitatively, this transient overshoot reaches a maximum relative error of approximately 6.2% against the analytical projection at $t \approx 0.31$s. However, the model quickly recovers, yielding an impressive overall Root Mean Square Error (RMSE) of only 0.0052 m/s across the entire computed domain. This condition is a relatively common characteristic encountered in the application of PINNs for modeling dynamic systems. PINNs models are trained by minimizing the differential equation residuals across the entire time domain simultaneously. Thus, the learning process does not always adhere to the causal structure of the system. Consequently, the model may learn the system's behavior at later times before fully comprehending its initial conditions. This can lead to discrepancies in the early dynamic phase, even though predictions in other parts of the domain appear reasonably accurate (Wang et al., 2022). Furthermore, the deviation phenomenon at early times is also associated with the spectral bias in neural networks, namely the tendency of neural networks to learn low-frequency components before capturing the high-frequency components of a function. In the context of physical systems, the initial dynamics frequently exhibit sharper changes compared to conditions approaching the steady state. Therefore, PINNs models tend to more readily learn the smoother and more stable portions of the solution rather than the segments featuring rapid changes (Wang et al., 2021). This phenomenon is often referred to as the PINNs paradox. Several studies also indicate that the performance of PINNs models is highly influenced by the training strategy, the distribution of collocation points, and the balance of the loss functions employed (Mishra & Molinaro, 2023).

The optimization dynamics of this training strategy can be directly observed through the loss function convergence curve presented in Figure 5. This logarithmic-scale visualization demonstrates how both the physics loss and the data loss simultaneously undergo a stable decline as the number of epochs increases. The significant reduction in the physics loss to a very small order of magnitude proves that the artificial neural network is not merely memorizing the observational data points (overfitting), but rather has computationally succeeded in embedding the structure of the governing differential equations into the model. The stability of the total loss curve in the final phase of training confirms that the value of the weighting parameter λ has facilitated the model in optimally balancing adherence to the laws of fluid mechanics motion and fidelity to limited empirical observations. By the end of the 5000 epochs, the physics residual loss rigorously minimized to an order of magnitude of 10^{-2} demonstrating computational precision.

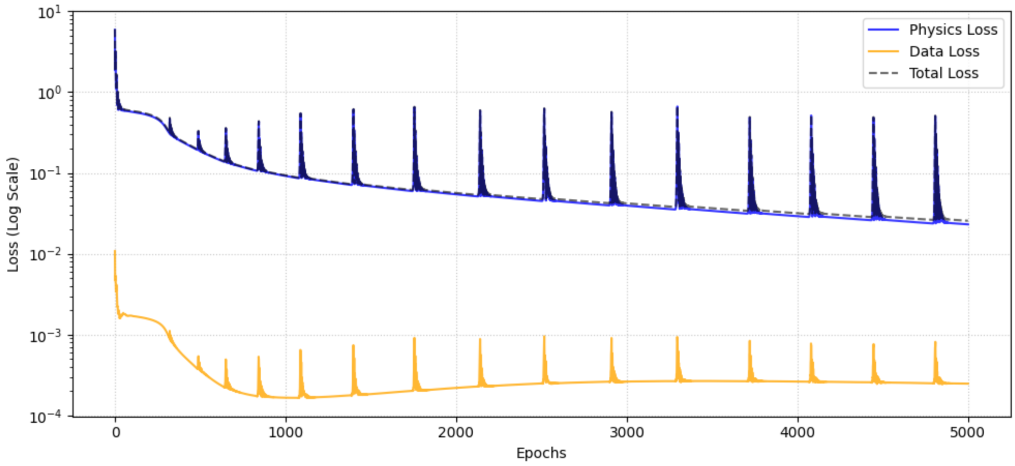

Figure 5. Loss function convergence during the PINNs training

On the other hand, while the PINNs predictions and the analytical solution have demonstrated convergence toward equilibrium at the terminal velocity (approximately 0.096 m/s), the experimental results exhibit a minor deceleration trend in the subsequent time phases. Based on the sensor data, the sphere does not perfectly align with the ideal steady-state condition characteristic of terminal velocity. Instead, the sphere continues to experience a gradual deceleration after the second measurement point. Specifically, the empirical velocity decays by approximately 29.0% from its initial transient peak down to 0.092 m/s at the final measurement point. This establishes a minor but consistent quantitative discrepancy of 0.004 m/s below the theoretically projected steady-state terminal velocity of 0.096 m/s. The physical validity of this deceleration is statistically evident from the uncertainty analysis of the repeated measurements. Visualization of the standard deviation range in the observational data indicates that the highest measurement variability occurs during the initial phase of motion ($t \approx 0.77$ s), representing the high sensitivity of transient dynamics to the particle's initial release conditions. Conversely, in the final time phase ($t \approx 5.16$ s), the uncertainty range narrows drastically, indicating an exceedingly high measurement consistency. While this empirical precision indicates that the persistent deceleration is not merely a random instrumental error, it also highlights the inherent constraints of the experimental setup. First, it is highly plausible that a longer tube trajectory might be required to observe whether the sphere eventually stabilizes at a new, lower terminal velocity. Second, this continuous deceleration could be strongly influenced by physical limitations during the process, such as unquantified near-wall effects or eccentric descent, which increase the drag force and are not fully encapsulated within the idealized analytical and PINNs models.

The magnitude of the deviation from the analytical assumption is explicitly visualized through the velocity residual plot in Figure 6. This residual graph represents the quantitative difference between the experimental velocity and the PINNs prediction results ($v_{\text{exp}} - v_{\text{pinn}}$). In contrast to the initial observation deviations, which are dominated by the inherent spectral bias factor of the neural network algorithm, the widening of the negative residual values at the final time measurement points demonstrates an anomalous force that is purely physical in nature. This plot confirms the presence of an extra drag force in the experiment that gradually reduces the sphere's velocity, far exceeding what is projected by the Stokes equation.

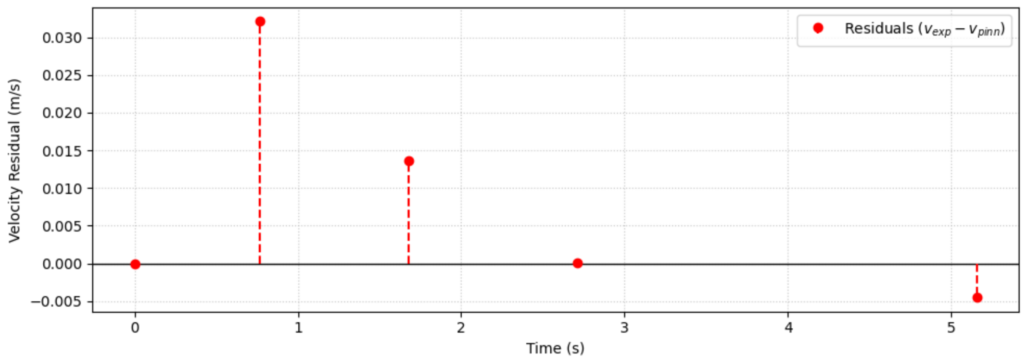

Figure 6. Velocity residual plot

The continuous deceleration observed in the experimental results can be explained through two fluid mechanics perspectives. First, as the sphere decelerates, the drag force it experiences becomes significantly larger compared to steady flow conditions. This increase in the drag coefficient is caused by a shift in the boundary-layer separation point, which occurs earlier or shifts upstream on the sphere's surface. This shift directly expands the wake area behind the sphere, which in turn increases the base pressure area, thereby augmenting the drag force and continuously amplifying the sphere's deceleration (Billa et al., 2025).

Second, this anomaly is also closely related to the microscopic characteristics of the specific experimental fluid utilized, which was commercial-grade glycerin subject to multiple experimental cycles. At the microscopic level, repeated usage introduces micro-impurities and potential structural variations, rendering the medium not perfectly homogeneous. In rheological literature, such conditions can trigger thixotropic properties. The continuous velocity deceleration occurs as a result of the ongoing restructuring process of the fluid's microstructure immediately in front of the falling solid object. The mechanism of random particle motion (Brownian motion) acts faster to restructure the fluid than the ability of the sphere's shear force to break it down. This dynamic process creates an increasingly large local resistance against the solid body, causing the sphere's velocity to continuously decelerate logarithmically and fail to maintain its terminal velocity (Koochi et al., 2023).

This comparative analysis yields significant implications for fluid dynamics modeling. The deviation observed between the PINNs predictions and the experimental data does not merely indicate a weakness in either method; rather, it illustrates that the PINNs approach can serve as a diagnostic tool to uncover hidden physical anomalies. The findings regarding this persistent deceleration pave the way for the development of future numerical models designed to be more sensitive to the complex dynamic properties of real-world fluids.

This study possesses several limitations. Experimental data acquisition relied solely on five infrared sensor points; consequently, the initial transient phase of the falling sphere was not recorded with high temporal resolution. Furthermore, the constructed PINNs modeling still utilizes a baseline architecture assuming constant viscosity (purely Newtonian flow). This model has not yet incorporated flexible time-dependent parameters to accommodate dynamic changes in viscosity as the object moves.

Conclusion

The comparison between Physics-Informed Neural Networks (PINNs) and experimental data from this study provides a more comprehensive understanding of the dynamics of a falling sphere in a fluid. Generally, the PINNs model proved reliable in predicting the trend of the sphere's motion until it reached a terminal velocity consistent with analytical theory. Nevertheless, this comprehensive comparison revealed two significant anomalies that highlight the limitations of both the PINNs architecture and the idealized analytical baseline. First, during the initial phase of motion, the PINNs model experienced a deviation in the form of an overshoot relative to the analytical solution due to the spectral bias effect. This occurs when the neural network is slow to adapt to highly abrupt changes in velocity. Second, in the middle to final time phase, the experimental data consistently demonstrated a deceleration in the sphere's velocity, a real-world dynamic that diverges from the constant terminal velocity projected by the analytical solution. This phenomenon eluded both analytical and PINNs predictions, indicating the emergence of an extra drag force caused by a shift in boundary-layer separation, as well as the thixotropic behavior of the fluid's microstructure. Overall, PINNs represent a highly promising approach to bridging the modeling of fundamental physical laws with computation. More than merely a predictive tool, the discrepancy between computational and experimental results actually proves that PINNs can be utilized as a diagnostic tool to detect the complexities of real-world fluids that deviate from ideal conditions. In order for this model architecture to better represent experimental reality, further research is strongly recommended to incorporate dynamic parameters to accommodate non-Newtonian effects. Furthermore, increasing the resolution of data acquisition by adding sensor points during the initial phase of the sphere's descent is also necessary to minimize the spectral bias effect during the network training process.

References

Syaifurrozaq, M., Marwoto, P., & Iswari, R. S. (2020). The determination of fluid viscosity using tracker-assisted falling ball viscosimeter. Journal of Physics: Conference Series, 1567(4), 042102. https://doi.org/10.1088/1742-6596/1567/4/042102

Akhyan, A., Ma'a, M., Irdam, F. A., Alvarez, A., Nugraha, N., & Nurkhamdi, N. (2025). Investigation of geometric effects on fluid viscosity using the falling ball method. Jurnal Polimesin, 23(5), 670–674. https://doi.org/10.30811/jpl.v23i5.7347

Barnes, H. A., Hutton, J. F., & Walters, K. (Eds.). (1989). *An introduction to rheology* (Vol. 3). Elsevier. https://doi.org/10.1016/B978-0-444-87469-6.50001-9

Beuchert, M. J., & Podladchikov, Y. Y. (2010). Viscoelastic mantle convection and lithospheric stresses. *Geophysical Journal International*, *183*(1), 35–63. https://doi.org/10.1111/j.1365-246X.2010.04708.x

Billa, P. K., Josyula, T., Tropea, C., & Mahapatra, P. S. (2025). Motion of a rigid sphere penetrating a deep pool. Journal of Fluid Mechanics, 1012, A5. https://doi.org/10.1017/jfm.2025.10166

Brizard, M., Megharfi, M., & Verdier, C. (2005). Estimation of falling ball viscosity measurement uncertainties. Metrologia, 42(4), 298–303. https://doi.org/10.1088/0026-1394/42/4/015

Chu, C.-R., Chiu, C.-L., & Yin, X.-X. (2024). Path instability of falling sphere induced by the near-wall effect. Physics of Fluids, 36(6), 063316. https://doi.org/10.1063/5.0212822

Cuomo, S., Di Cola, V. S., Giampaolo, F., Rozza, G., Raissi, M., & Piccialli, F. (2022). Scientific machine learning through physics–informed neural networks: Where we are and what's next. Journal of Scientific Computing, 92(3), 88. https://doi.org/10.1007/s10915-022-01939-z

Fowler, E., McDevitt, C. J., & Roy, S. (2024). Physics-informed neural network simulation of thermal cavity flow. Scientific Reports, 14(1), 15203. https://doi.org/10.1038/s41598-024-65664-3

Goodfellow, I., Bengio, Y., & Courville, A. (2016). Deep learning. MIT Press. https://mitpress.mit.edu/9780262035613/deep-learning/

Kaliappan, S., Raj Kamal, M. D., Joseph Manuel, D., Balaji, V., & Murugan, P. (2022). Viscous flow and its effect. In S. K. Kumar & N. S. Radhakrishnan (Eds.), Handbook of research on aspects and applications of incompressible and compressible aerodynamics (pp. 129–141). IGI Global. https://doi.org/10.4018/978-1-6684-4230-2.ch006

Karniadakis, G. E., Kevrekidis, I. G., Lu, L., Perdikaris, P., Wang, S., & Yang, L. (2021). Physics-informed machine learning. Nature Reviews Physics, 3(6), 422–440. https://doi.org/10.1038/s42254-021-00314-5

Khain, T., Scheibner, C., Fruchart, M., & Vitelli, V. (2022). Stokes flows in three-dimensional fluids with odd and parity-violating viscosities. Journal of Fluid Mechanics, 934. https://doi.org/10.1017/jfm.2021.1079

Koochi, H., Mac Intyre, J., Korhonen, M., Puisto, A., Maleki-Jirsaraei, N., & Alava, M. J. (2023). Interaction between a free-falling sphere and structure dynamics in a heterogeneous thixotropic fluid. Physics of Fluids, 35(8), 083108. https://doi.org/10.1063/5.0158738

Mendez, Y. (2011). A flow model for the settling velocities of non spherical particles in creeping motion. Journal of Applied Fluid Mechanics, 4(4), 65–75. https://doi.org/10.36884/jafm.4.04.11948

Mishra, S., & Molinaro, R. (2023). Estimates on the generalization error of physics-informed neural networks (PINNs) for approximating a class of inverse problems for PDEs. arXiv preprint arXiv:2007.01138. https://doi.org/10.48550/arXiv.2007.01138

Mitev, P., Tashev, A., & Stoyanov, Y. (2025). Design and construction of an engine oil viscosity meter with electronic control. Engineering Proceedings, 100(1). https://doi.org/10.3390/engproc2025100055

Protopapas, E., Vafeas, P., & Hadjinicolaou, M. (2025). Stokes flow around a paraboloid of revolution: Analytical treatment in an unbounded domain. Physics of Fluids, 37(10). https://doi.org/10.1063/5.0293259

Raissi, M., Perdikaris, P., & Karniadakis, G. E. (2019). Physics-informed neural networks: A deep learning framework for solving forward and inverse problems involving nonlinear partial differential equations. Journal of Computational Physics, 378, 686–707. https://doi.org/10.1016/j.jcp.2018.10.045

Ren, Z., Zhou, S., Liu, D., & Liu, Q. (2025). Physics-informed neural networks: A review of methodological evolution, theoretical foundations, and interdisciplinary frontiers toward next-generation scientific computing. Applied Sciences, 15(14), 8092. https://doi.org/10.3390/app15148092

Rückert, M. (2023). *Reproducibility of falling body viscometry* (Doctoral dissertation, RWTH Aachen University). Shaker Verlag. https://doi.org/10.18154/RWTH-2023-06683

Salomone, H. D., Olivieri, N. A., Véliz, M. E., & Raviola, L. A. (2018). A non-traditional fluid problem: Transition between theoretical models from Stokes' to turbulent flow. European Journal of Physics, 39(3). https://doi.org/10.1088/1361-6404/aaa34b

Wang, S., Sankaran, S., & Perdikaris, P. (2022). Respecting causality is all you need for training physics-informed neural networks. arXiv preprint arXiv:2203.07404. https://doi.org/10.48550/arXiv.2203.07404

Wang, S., Wang, H., & Perdikaris, P. (2021). On the eigenvector bias of Fourier feature networks: From regression to solving multi-scale PDEs with physics-informed neural networks. Computer Methods in Applied Mechanics and Engineering, 384, 113938. https://doi.org/10.1016/j.cma.2021.113938

White, F. M. (2011). *Fluid mechanics* (7th ed.). McGraw-Hill Education. ISBN 978-0-07-352934-9

White, F. M., & Xue, H. (2021). *Fluid mechanics* (9th ed.). McGraw-Hill Education. ISBN 978-1-260-44655-5